Eur. Phys. J. B (2015) 88: 93
DOI: 10.1140/epjb/e2015-50746-9

THE EUROPEAN PHYSICAL JOURNAL B

Regular Article

First-principle investigation of half-metallic ferromagnetism in octahedrally bonded Cr-doped rock-salt SrS, SrSe, and SrTe

Bendouma Doumi[1,2,a], Allel Mokaddem[3], Lahouari Temimi[4], Nadir Beldjoudi[5], Mohammed Elkeurti[1], Fethallah Dahmane[2,6], Adlane Sayede[7], Abdelkader Tadjer[2], and Mustapha Ishak-Boushaki[8]

[1] Faculty of Sciences, Department of Physics, Dr. Tahar Moulay University of Saïda, 20000 Saïda, Algeria
[2] Modelling and Simulation in Materials Science Laboratory, Physics Department, Djillali Liabes University of Sidi Bel-Abbes, 22000 Sidi Bel-Abbes, Algeria
[3] Faculty of Physics, Department of Materials and Components, U.S.T.H.B., Algiers, Algeria
[4] Mohamed Boudiaf University of Science and Technology of Oran, 31000 Oran, Algeria
[5] Faculty of Physics, Theoretical Physics Laboratory, U.S.T.H.B, Algiers, Algeria
[6] Institut des Sciences et Technologies, Département sciences de la matière, Centre Universitaire de Tissemsilt, 38000 Tissemsilt, Algeria
[7] Unité de Catalyse et Chimie du Solide (UCCS), UMR CNRS 8181, Faculté des Sciences, Université d'Artois, Rue Jean Souvraz, SP 18, 62307 Lens, France
[8] Faculty of Physics, U.S.T.H.B., Algiers, Algeria

Received 25 October 2014 / Received in final form 14 February 2015
Published online 8 April 2015 –

Abstract. We have investigated the electronic structure and half-metallic ferromagnetism of $Sr_{1-x}Cr_xZ$ (Z = S, Se, and Te) in rock-salt structure at concentrations x (x = 0.125, 0.25, 0.5, 0.75 and 0.875) of Cr, using first-principles calculations of density functional theory. The electronic and magnetic properties show that $Sr_{1-x}Cr_xZ$ (Z = S and Se) at x = 0.125, 0.25, 0.5, 0.75 and $Sr_{1-x}Cr_xTe$ at all concentrations are half-metallic ferromagnets (HMF) with spin polarization of 100% and total magnetic moments of $4\mu_B$ per Cr atom, whereas the HMF character destroyed for $Sr_{1-x}Cr_xZ$ (Z = S and Se) at x = 0.875. The integrals Bohr magneton of total magnetic moments confirm the half-metallic ferromagnetic behavior of $Sr_{1-x}Cr_xZ$. We have found that the ferromagnetic state is stable by the 3*d*-*eg* (Cr) partially filled states associated with the double-exchange mechanism. Therefore, the $Sr_{1-x}Cr_xS$, $Sr_{1-x}Cr_xSe$, and $Sr_{1-x}Cr_xTe$ at low concentration are predicted to be new potential candidates for spintronic applications.

1 Introduction

Spintronics (spin transport electronics or spin-based electronics) is a new generation of microelectronics, which exploits the spin of charge carriers in the emerging field of promising materials for spin-based multifunctional devices [1–3]. Hence, the diluted magnetic semiconductors (DMSs) attracted the interest of researchers, since they represent new properties of promising materials for practical applications in spintronic devices. In the recent years, extensive theoretical [4–13] and experimental [14–19] researches have been focused on the investigation and the discovery of ferromagnetism in the DMSs-based II-VI and III-V semiconductors in the intention to use them for spin injection in the spintronic applications. These materials are promising systems to explore DMSs because they are characterized by two features needed for spintronic applications; the Curie temperature above the room temperature and half-metallic behavior [20]. However, the expected advantage of spintronic devices over the conventional electronic ones would be nonvolatility, increased data processing speed, increased transistor density and decreased power consumption [21].

The II-VI (II = Be, Mg, Ca, Sr, and Ba; VI = O, S, Se, and Te) alkaline-earth-chalcogenides are very important semiconductors with large band gaps and valence-band widths [22]. They form closed-shell ionic systems crystallized in the rock-salt NaCl-type (B1) crystal structure at ambient conditions, except for BeO and MgTe (crystallized in the wurtzite structure) and the beryllium chalcogenides (crystallized in the zinc-blende structure) [23–25]. The SrZ (Z = S, Se, and Te) strontium chalcogenides have attracted increasing interest because they are good materials for technological applications in the area of catalysis, microelectronics, luminescent devices, radiation dosimetry, fast high resolution optically stimulated luminescence imaging, and infrared sensitive devices [26–28]. Recently, several theoretical studies have been performed in order to investigate the half-metallic ferromagnetic properties in the alkaline-earth-chalcogenides doped with nonmagnetic elements such as (B, C, and N)-doped AeSr (Ae = Mg, Ca, Sr, and Ba) [29], (N, P, As, and Sb)-doped AeS (Ae = Mg, Ca, and Sr) [30], and $AeS_{1-x}M_x$ (Ae = Mg, Ca, and Sr; M = C, Si, Ge, and Sn) [31].

[a] e-mail: bdoummi@yahoo.fr

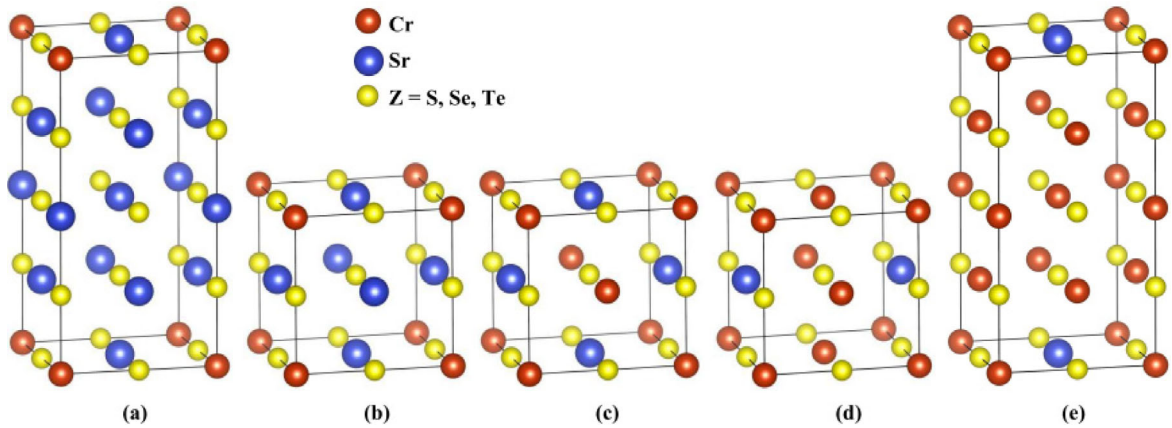

Fig. 1. The crystal structures of $Sr_{1-x}Cr_xZ$ (Z = S, Se, and Te): (a) $Sr_{0.875}Cr_{0.125}Z$ with $x = 0.125$, (b) $Sr_{0.75}Cr_{0.25}Z$ with $x = 0.25$, (c) $Sr_{0.5}Cr_{0.5}Z$ with $x = 0.5$, (d) $Sr_{0.25}Cr_{0.75}Z$ with $x = 0.75$, and (e) $Sr_{0.125}Cr_{0.875}Z$ with $x = 0.875$.

To the best of our knowledge, there are no experimental and theoretical studies of electronic and magnetic properties for Cr-doped SrZ (Z = S, Se, and Te). Therefore, in this paper, we will investigate the half-metallic ferromagnetic properties of $Sr_{1-x}Cr_xZ$ (Z = S, Se, and Te) at concentrations $x = 0.125$, 0.25, 0.5, 0.75 and 0.875 based on simple model structures of ordered supercells of 16 and 8 atoms, using the first-principle full-potential linearized augmented plane-wave method with the generalized gradient approximation functional of Wu and Cohen (GGA-WC) [32].

2 Method of calculations and optimization of structures

The calculations of the present study are performed in the framework of the density functional theory [33,34]. We have employed the full-potential linearized augmented plane-wave method as implemented in the WIEN2k code [35]. The generalized gradient approximation functional of Wu and Cohen (GGA-WC) [32] was used for the exchange correlation potential. The SrS, SrSe, and SrTe semiconductors have rock-salt (B1) structure with space group of 225 (Fm-$3m$), where the Sr atom is located at (0, 0, 0) and (Z = S, Se and Te) atom at (0.5, 0.5, 0.5) position, with the experimental lattice constant of 6.024 Å [36], 6.236 Å [37], and 6.66 Å [38] for SrS, SrSe, and SrTe, respectively. The concentrations $x = 0.125$ and 0.25 are realized by substituted of one Sr cation site at position (0, 0, 0) by one Cr atom in supercell of 16 and 8 atoms, respectively. We get the $Sr_{0.875}Cr_{0.125}Z$ for $x = 0.125$ with tetragonal structure of space group 123 ($P4/mmm$) and $Sr_{0.75}Cr_{0.25}Z$ for $x = 0.25$ with cubic structure of space group 221 (Pm-$3m$). We obtain the $Sr_{0.5}Cr_{0.5}Z$ supercell of 8 atoms for concentration $x = 0.5$ by substituted of two Sr cation sites with two Cr atoms. The concentrations $x = 0.75$ and 0.875 are obtained by replacing three and seven Sr cation sites by three and seven Cr atoms in supercell of 8 and 16 atoms, respectively. We acquired the $Sr_{0.25}Cr_{0.75}Z$ for $x = 0.75$ with cubic structure of space group 221 (Pm-$3m$) and $Sr_{0.125}Cr_{0.875}Z$ for $x = 0.875$ with tetragonal structure of space group 123 ($P4/mmm$) as shown in Figure 1.

We take the averages of non-overlapping muffin-tin radii (R_{MT}) of Sr, S, Se, Te, and Cr in such a way that the muffin-tin spheres do not overlap. We have expanded the wave functions in the interstitial region to plane waves with a cutoff of $K_{max} = 8.0/R_{MT}$ (where K_{max} is the magnitude of the largest K vector in the plane wave and R_{MT} is the average radius of the muffin-tin spheres), and the maximum value for partial waves inside the atomic sphere was $l_{max} = 10$. While, the charge density was Fourier expanded up to $G_{max} = 14$ a.u.$^{-1}$, where G_{max} is the largest vector in the Fourier expansion. For the sampling of the Brillouin zone, we have used the Monkhorst-Pack mesh [39,40] of $(4 \times 4 \times 4)$ for SrZ, $Sr_{0.75}Cr_{0.25}Z$ and $Sr_{0.25}Cr_{0.75}Z$, $(4 \times 4 \times 2)$ for $Sr_{0.875}Cr_{0.125}Z$ and $Sr_{0.125}Cr_{0.875}Z$, and $(4 \times 4 \times 3)$ for $Sr_{0.5}Cr_{0.5}Z$, where the self-consistent convergence of the total energy was at 0.1 mRy.

The variations of total energies as a function of equilibrium volumes are fitted with the empirical Murnaghan's equation of state [41] to determine the equilibrium lattice constants for SrZ and $Sr_{1-x}Cr_xZ$ (Z = S, Se, and Te) compounds. Our results, various theoretical [42,43] and experimental [36–38] data are given in Table 1. The lattice constants of SrS, SrSe, and SrTe semiconductors are very close to the experimental values [36–38], and stay in good agreement with theoretical calculations [42,43] of generalized gradient approximation of Perdew, Burke, and Ernzerhof (GGA-PBE) [44]. On the other hand, due to better performance of GGA-WC approximation for structural optimization [45–47], resulting from the fourth-order gradient expansion of exchange-correlation functional [32,46], our results with GGA-WC are better than the theoretical calculations [42,43] of GGA-PBE method as depicted in Table 1. Besides, there is some decrease in the lattice constants with increasing Cr concentration for ternary $Sr_{1-x}Cr_xZ$ (Z = S, Se, and Te) compared to the binary SrZ (Z = S, Se, and Te) compounds because the ionic radius of Cr is smaller than that of Sr atom. We can notice

Table 1. Calculation of lattice constants (a) for SrZ, and $Sr_{1-x}Cr_xZ$ (Z = S, Se, and Te) at concentrations $x = 0.125$, 0.25, 0.5, 0.75, and 0.875.

Compound	Concentration (x)	a (Å)	
$Sr_{1-x}Cr_xS$	0	5.988	6.024[a], 6.05[d], 6.065[e]
	0.125	5.883	
	0.25	5.791	
	0.5	5.579	
	0.75	5.341	
	0.875	5.229	
$Sr_{1-x}Cr_xSe$	0	6.204	6.236[b], 6.29[d], 6. 303[e]
	0.125	6.110	
	0.25	6.016	
	0.5	5.808	
	0.75	5.566	
	0.875	5.462	
$Sr_{1-x}Cr_xTe$	0	6.621	6.660[c], 6.71[d], 6.735[e]
	0.125	6.517	
	0.25	6.424	
	0.5	6.211	
	0.75	5.955	
	0.875	5.837	

[a] Experimental value from reference [36]. [b] Experimental value from reference [37]. [c] Experimental value from reference [38]. [d] Theoretical values from reference [42]. [e] Theoretical values from reference [43].

that there are no experimental and theoretical GGA-WC calculations of lattice constants for $Sr_{1-x}Cr_xZ$ compounds to compare with our results. As well, the computed lattice constants are used in the next calculations of electronic and magnetic properties of $Sr_{1-x}Cr_xZ$ (Z = S, Se, and Te).

3 Results and discussions

3.1 Electronic properties

3.1.1 Band structure with half-metallic gap

The spin-polarized band structures along high-symmetry directions in the first Brillouin zone for $Sr_{1-x}Cr_xS$, $Sr_{1-x}Cr_xSe$, and $Sr_{1-x}Cr_xTe$ at concentration $x = 0.125$ are displayed in Figures 2, 3 and 4, respectively. They exhibit half-metallic ferromagnetic behavior with the majority-spin bands being metallic and the minority-spin bands being semiconducting. In addition, the band structures show that majority-spin bands are more in number than the minority-spin bands due to the p-d exchange interaction, this creates the half-metallic ferromagnetic band gaps (E_g) and half-metallic gaps (G_{HM}) in the minority-spin bands. These comportments are found for $Sr_{1-x}Cr_xZ$ (Z = S, Se, and Te) at ($x = 0.125$, 0.25, 0.5, and 0.75) and $Sr_{1-x}Cr_xTe$ at concentration $x = 0.875$ (Fig. 7), while the $Sr_{1-x}Cr_xZ$ (Z = S and Se) at $x = 0.875$ compounds reveal metallic nature for majority and minority spin as shown in Figures 5 and 6.

Moreover, the half-metallic gap is a very significant parameter in determining the importance of the diluted magnetic semiconductor, which is defined as the minimum

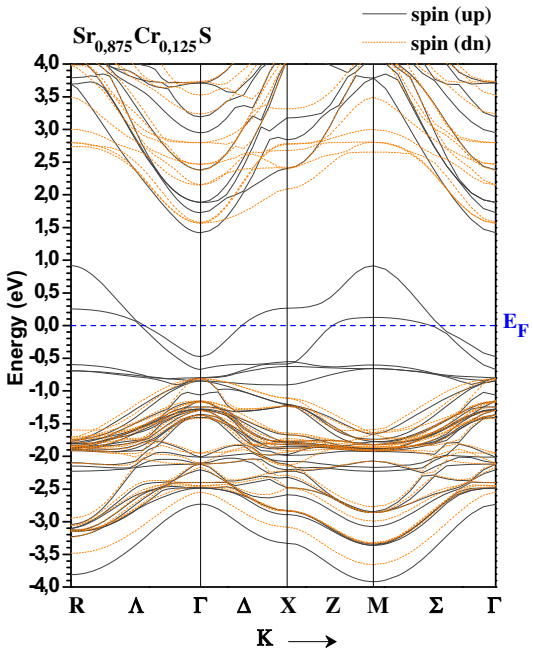

Fig. 2. Spin-polarized band structures of majority spin (up) and minority spin (dn) for $Sr_{0.875}Cr_{0.125}S$. The Fermi level is set to zero (horizontal dotted line).

between the lowest energy of majority (minority)-spin conduction bands with respect to the Fermi level and the absolute value of the highest energy of majority (minority)-spin valence bands [48,49]. The calculations of E_g (eV) and G_{HM} (eV) for minority-spin channels are given in Table 2. The $Sr_{1-x}Cr_xS$, $Sr_{1-x}Cr_xSe$, and $Sr_{1-x}Cr_xTe$ compounds at concentration $x = 0.125$ have direct half-metallic

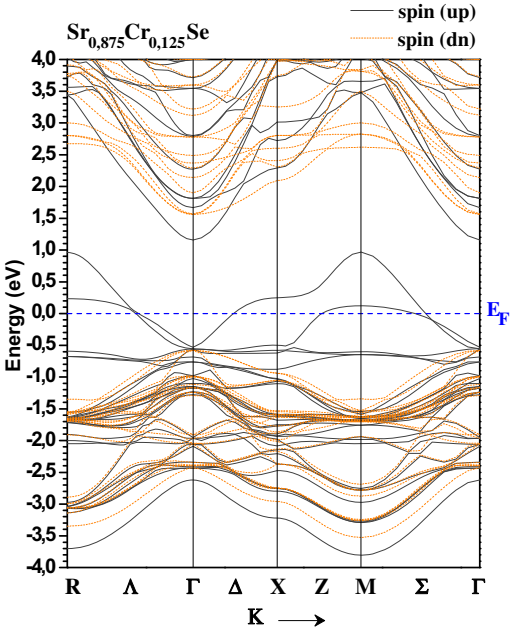

Fig. 3. Spin-polarized band structures of majority spin (up) and minority spin (dn) for $Sr_{0.875}Cr_{0.125}Se$. The Fermi level is set to zero (horizontal dotted line).

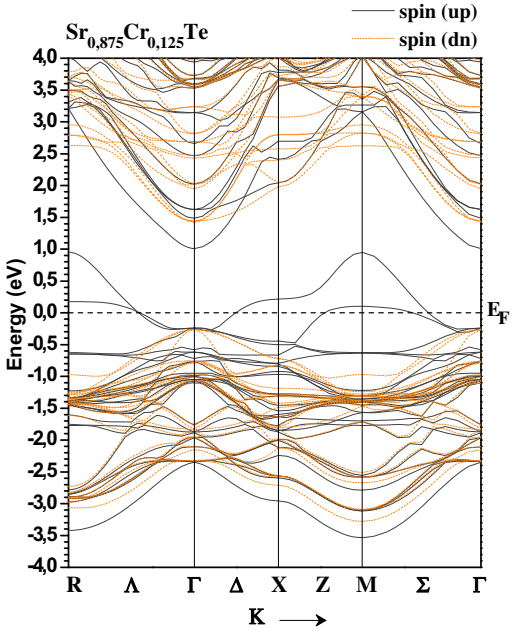

Fig. 4. Spin-polarized band structures of majority spin (up) and minority spin (dn) for $Sr_{0.875}Cr_{0.125}Te$. The Fermi level is set to zero (horizontal dotted line).

ferromagnetic (HMF) gaps because the E_g is located at the Γ point of the Brillouin zone. For $Sr_{1-x}Cr_xZ$ the localized $3d$ (Cr) bands broadening as the concentration of Cr impurity increases, and thus the HMF gap decreases with increasing Cr concentration. Figures 5 and 6 of $Sr_{1-x}Cr_xS$ and $Sr_{1-x}Cr_xSe$ at higher concentration $x = 0.875$ show that the minority-spin conduction bands dominate the Fermi level due to strong broadening of $3d$ (Cr) orbitals in the gap and therefore the half-metallic character destroyed. In this case the majority-spin and minority-spin bands are metallic in nature, which means that $Sr_{0.125}Cr_{0.875}S$ and $Sr_{0.125}Cr_{0.875}Se$ are metallic materials. In contrast the $Sr_{1-x}Cr_xTe$ at $x = 0.875$ (Fig. 7) reveals that majority-spin and minority-spin bands are metallic and semiconductor, respectively, this implies that $Sr_{0.125}Cr_{0.875}Te$ exhibits a half-metallic ferromagnetic behavior. Also, Table 2 shows a nonlinear decrease in half-metallic ferromagnetic gaps and HM gaps of $Sr_{1-x}Cr_xZ$ with increasing of concentration (x) of Cr due to the local electric field and local strain introduced by the magnetic of Cr impurities [13].

Furthermore the HM gap (G_{HM}) decreases from $Sr_{0.875}Cr_{0.125}S$ to $Sr_{0.875}Cr_{0.125}Se$ to $Sr_{0.875}Cr_{0.125}Te$ as shown in Figures 2–4, and it is situated between the highest energy of minority-spin valence bands and Fermi level. Especially, the maximum of the valence bands that contains the p (S, Se, and Te) states moves towards the Fermi level from S to Se to Te, and hence the half-metallic gap decreases from $Sr_{0.875}Cr_{0.125}S$ to $Sr_{0.875}Cr_{0.125}Se$ to $Sr_{0.875}Cr_{0.125}Te$ as the energy level of p (Z) states increases from $3p$ (S) to $4p$ (Se) to $5p$ (Te). Further, the $Sr_{1-x}Cr_xS$ at low concentration $x = 0.125$ has a wider HM gap, which is located between Fermi level (0 eV) and the top of minority-spin valence bands (0.815 eV) while the bottom of minority-spin conduction bands is at 1.566 eV. Therefore, the smallest gaps for generating a hole and electron in minority-spin are 0.815 and 1.566 eV, respectively, as consequence the minimal energy gap for a spin excitation is 0.815 eV, which corresponds to a HM gap of 0.815 eV. Thus, the large HM gap shapes a true half-metallic ferromagnet, and makes $Sr_{0.875}Cr_{0.125}S$ a best potential material than the other $Sr_{1-x}Cr_xZ$ (Z = S, Se, and Te) at $x = 0.25$, 0.5, 0.75 and $Sr_{0.125}Cr_{0.875}Te$ compounds for spintronic applications.

Table 2. Calculated half-metallic ferromagnetic band gap (E_g) and half-metallic gap (G_{HM}) of minority-spin bands for $Sr_{1-x}Cr_xS$ and $Sr_{1-x}Cr_xSe$ at concentrations ($x = 0.125$, 0.25, 0.5, and 0.75) and $Sr_{1-x}Cr_xTe$ at ($x = 0.125$, 0.25, 0.5, 0.75, and 0.875).

Compound	Concentration (x)	E_g (eV)	G_{HM} (eV)
$Sr_{1-x}Cr_xS$	0.125	2.381	0.815
	0.25	2.081	0.777
	0.5	1.796	0.763
	0.75	1.378	0.032
$Sr_{1-x}Cr_xSe$	0.125	2.141	0.580
	0.25	1.870	0.498
	0.5	1.651	0.761
	0.75	1.241	0.272
$Sr_{1-x}Cr_xTe$	0.125	1.687	0.263
	0.25	1.456	0.186
	0.5	1.246	0.348
	0.75	0.824	0.409
	0.875	0.652	0.139

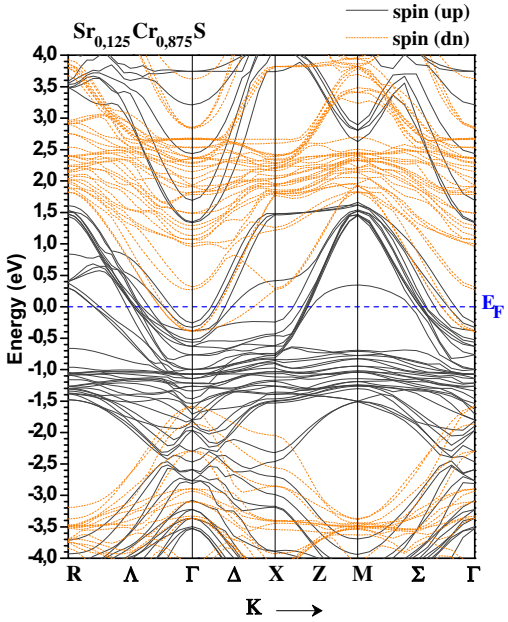

Fig. 5. Spin-polarized band structures of majority spin (up) and minority spin (dn) for $Sr_{0.125}Cr_{0.875}S$. The Fermi level is set to zero (horizontal dotted line).

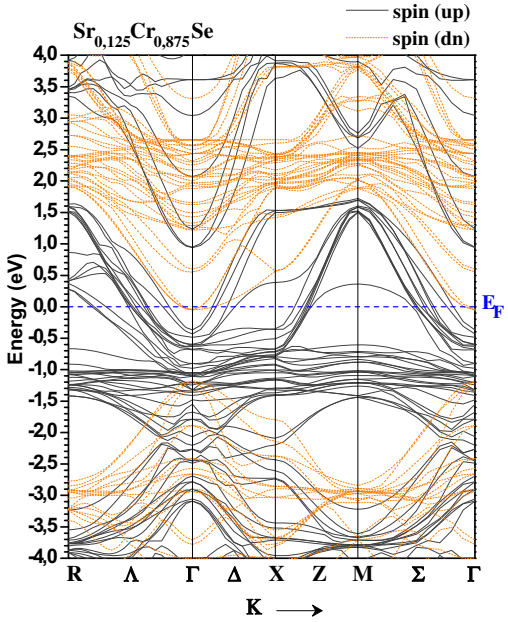

Fig. 6. Spin-polarized band structures of majority spin (up) and minority spin (dn) for $Sr_{0.125}Cr_{0.875}Se$. The Fermi level is set to zero (horizontal dotted line).

3.1.2 Density of states

The calculated of spin-polarized total and partial densities of states (DOS) for $Sr_{0.875}Cr_{0.125}S$, $Sr_{0.875}Cr_{0.125}Se$, and $Sr_{0.875}Cr_{0.125}Te$ are given in Figures 8–10. They depict half-metallic behavior resulted from metallic majority spin and semiconducting minority spin that leads to spin polarization of 100% at Fermi level. We found a similar behavior for $Sr_{1-x}Cr_xZ$ (Z = S, Se, and Te) at concentrations $x = 0.125$, 0.25, 0.5, 0.75 and $Sr_{1-x}Cr_xTe$ at $x = 0.875$. Besides, the effect of the octahedral crystal field formed by surrounding (S, Se, and Te) ligands splits the five-fold degenerate $3d$ states of the free Cr ion into twofold generate threefold degenerate low-lying $t_{2g}(d_{xy}d_{xz}$ and $d_{yz})$ and high-lying $e_g(d_{z^2}$ and $d_{x^2-y^2})$ symmetry states. Also, the energy of e_g states is higher than the energy of t_{2g} states, indicating that Cr ion is situated in the octahedral surroundings.

Figures 8–10 of DOS show that the lower part of valence bands of two spin channels originated from the contributions of p (S, Se, and Te) states, and the upper part of valence bands of the majority spin around the Fermi level are mainly dominated by the peak of $3d$ (Cr) and the p (S, Se, and Te) states. Then, we depicted that the top of valence bands of majority spin and the bottom of conduction bands of the minority spin are principally formed by the strong hybridizations between $3d$ (Cr) and p (S, Se, and Te) band carriers of host semiconductors. This creates some bands in the host valence bands; the bonding (t^b) and the non-bonding (e) states in the valence bands, and the anti-bonding states (t^a) in the band gap. Further, the anti-bonding states are characterized by the strong hybridizations between p (S, Se, and Te) and $3d$-e_g (Cr) partially filled states that cross the Fermi level. We understand that the stabilization of ferromagnetism is explained by a double-exchange mechanism [50] when the $3d$-e_g (Cr) localized anti-bonding states are partially occupied. This suggestion for ferromagnetism of octahedrally bonded Cr in the $Sr_{1-x}Cr_xZ$ (Z = S, Se, and Te) doping systems is analogous to the one proposed by Sato et al. [51–53] for ferromagnetism in the case of tetrahedrally bonded of transition metals (TM)-doped III-V and II-VI semiconductors when the $3d$-t_{2g} (TM) anti-bonding states are partially occupied.

3.2 Magnetic properties

3.2.1 Magnetic moments

The calculated total and local magnetic moments per Cr atom within the muffin-tin spheres of the relevant (Sr, S, Se, Te, and Cr) atoms and in the interstitial sites for $Sr_{1-x}Cr_xS$, $Sr_{1-x}Cr_xSe$, and $Sr_{1-x}Cr_xTe$ at different concentrations are listed in Table 3. The Cr atom contributes two electrons to bonding of host valence band semiconductor resulting in Cr^{+2} ion, as consequence the electronic configuration of $3d$ (Cr) in $Sr_{1-x}Cr_xZ$ is $(d^4 - t_{2g}^3 e_g^1)$. According to the Hund's rule, the $3d$ (Cr) orbitals are empty minority spin whereas they are partially filled by four electrons for majority spin. For each of $Sr_{1-x}Cr_xS$ and $Sr_{1-x}Cr_xSe$ at concentrations $x = 0.125, 0.25, 0.5, 075$ and $Sr_{1-x}Cr_xTe$ at $x = 0.125$, 0.25, 0.5, 075, and 0.875 materials, the four electrons provide a total magnetic moment of $4\mu_B$ (μ_B is the Bohr magneton) per Cr atom, this confirms the half-metallic behavior of $Sr_{1-x}Cr_xZ$ systems. In distinguish, the $Sr_{1-x}Cr_xS$ and $Sr_{1-x}Cr_xSe$ at higher concentration $x = 0.875$ are metallic (Figs. 5 and 6), which is

Table 3. Calculated total and local magnetic moments per Cr atom (in Bohr magneton μ_B) within the muffin-tin spheres and in the interstitial sites for $Sr_{1-x}Cr_xZ$ (Z = S, Se, and Te) at concentrations $x = 0.125$, 0.25, 0.5, 0.75, and 0.875.

Compound	Concentration (x)	Tot. (μ_B)	Cr (μ_B)	Sr (μ_B)	Z (μ_B)	Interstitial (μ_B)
$Sr_{1-x}Cr_xS$	0.125	4.000	3.891	0.004	−0.221	0.326
	0.25	4.002	3.821	0.007	−0.171	0.345
	0.5	4.001	3.784	0.008	−0.108	0.317
	0.75	4.002	3.735	0.004	−0.053	0.316
	0.875	3.973	3.614	0.002	−0.037	0.394
$Sr_{1-x}Cr_xSe$	0.125	4.000	3.919	0.003	−0.277	0.355
	0.25	4.003	3.847	0.005	−0.228	0.379
	0.5	4.002	3.816	0.006	−0.154	0.334
	0.75	4.004	3.776	0.005	−0.095	0.318
	0.875	3.986	3.726	0.001	−0.083	0.342
$Sr_{1-x}Cr_xTe$	0.125	4.000	3.977	−0.003	−0.250	0.278
	0.25	4.002	3.921	0.003	−0.224	0.302
	0.5	4.002	3.888	0.004	−0.198	0.311
	0.75	4.001	3.811	0.003	−0.136	0.323
	0.875	4.000	3.787	0.001	−0.117	0.329

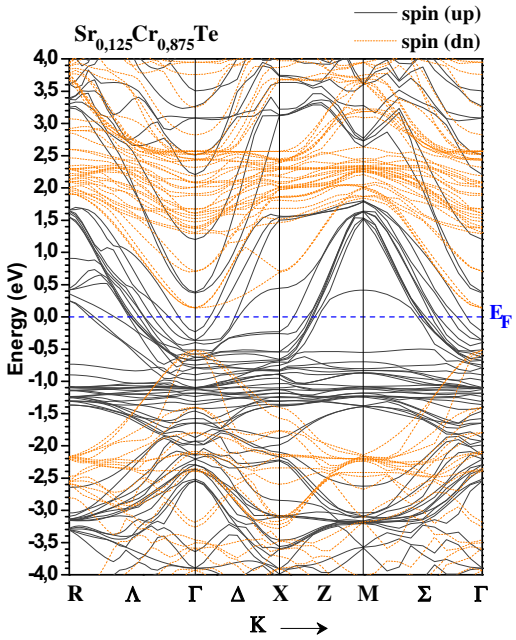

Fig. 7. Spin-polarized band structures of majority spin (up) and minority spin (dn) for $Sr_{0.125}Cr_{0.875}Te$. The Fermi level is set to zero (horizontal dotted line).

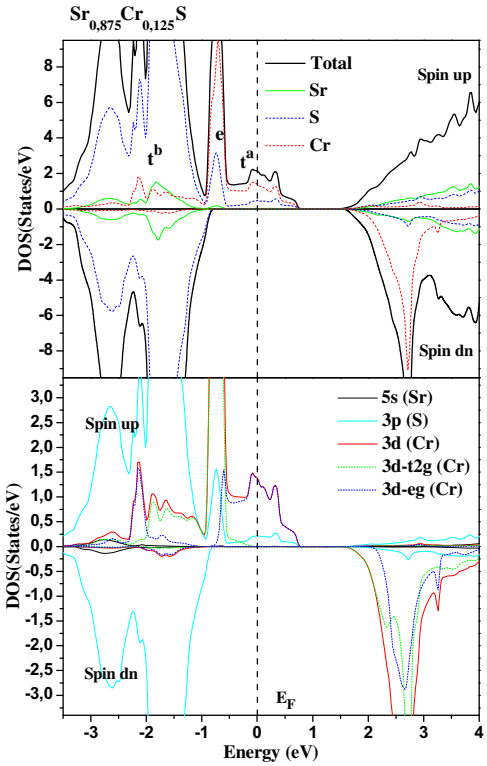

Fig. 8. Spin-polarized total and partial DOS of (5s) of Sr, (3p) of S, and (3d, 3d-t_{2g}, 3d-e_g) of Cr in supercell of $Sr_{0.875}Cr_{0.125}S$. The Fermi level is set to zero (vertical dotted line).

reasonable that their magnetic moments are not integers as shown in Table 3. The major contribution of total magnetic moment comes from the local magnetic moment of Cr, which is smaller than the predicted Hund's rule value of $4\mu_B$ due to the large p-d hybridization. The negative local magnetic moments of (Z = S, Se, and Te) reveal the anti-ferromagnetic interaction between Cr magnetic spins and the induced magnetizations at S, Se, and Te anions, while the positive magnetic polarizations at the Sr sites show the ferromagnetic interaction between Sr and Cr spins. Also, the anti-ferromagnetic interaction is initialized between Sr and Cr spins for $Sr_{1-x}Cr_xTe$ at concentration $x = 0.125$.

3.2.2 Exchange coupling

Finally, the half-metallic ferromagnetic band structures can be used to compute two important parameters, the s-d exchange constant $N_0\alpha$ (conduction band) and the p-d exchange constant $N_0\beta$ (valence band), these parameters can be determined directly from the following

Table 4. Calculated conduction and valence band-edge spin-splitting ΔE_c and ΔE_v, and exchange constants $N_0\alpha$ and $N_0\beta$ for $Sr_{1-x}Cr_xS$ and $Sr_{1-x}Cr_xSe$ at concentrations $x = 0.125$, 0.25, 0.5, 0.75 and $Sr_{1-x}Cr_xTe$ at $x = 0.125$, 0.25, 0.5, 0.75, 0.875.

Compound	Concentration (x)	ΔE_c (eV)	ΔE_v (eV)	$N_0\alpha$	$N_0\beta$
$Sr_{1-x}Cr_xS$	0.125	0.147	–0.339	0.588	–1.356
	0.25	0.379	–0.031	0.758	–0.062
	0.5	0.281	–0.149	0.281	–0.149
	0.75	1.275	–0.932	0.850	–0.621
$Sr_{1-x}Cr_xSe$	0.125	0.402	–0.048	1.608	–0.192
	0.25	0.781	–0.024	1.562	–0.048
	0.5	0.225	–0.035	0.225	–0.035
	0.75	0.640	–0.461	0.427	–0.307
$Sr_{1-x}Cr_xTe$	0.125	0.414	–0.024	1.656	–0.096
	0.25	0.959	–0.036	1.918	–0.072
	0.5	0.264	–0.051	0.264	–0.051
	0.75	0.141	–0.024	0.094	–0.016
	0.875	0.230	–0.276	0.131	–0.158

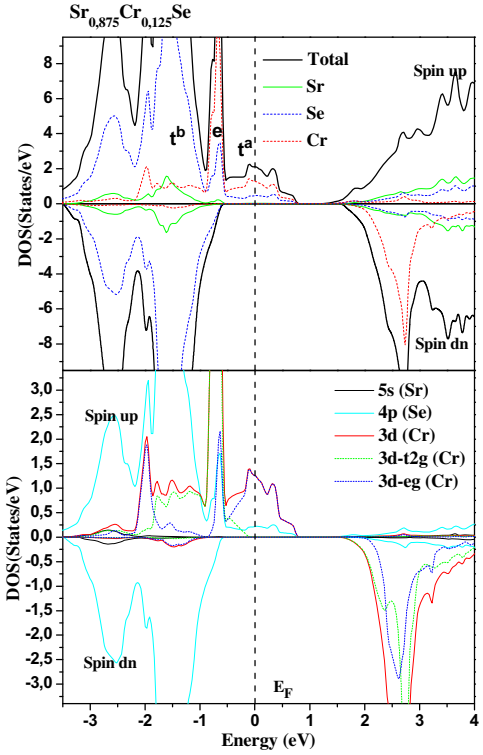

Fig. 9. Spin-polarized total and partial DOS of (5s) of Sr, (4p) of Se, and (3d, 3d-t_{2g}, 3d-e_g) of Cr in supercell of $Sr_{0.875}Cr_{0.125}Se$. The Fermi level is set to zero (vertical dotted line).

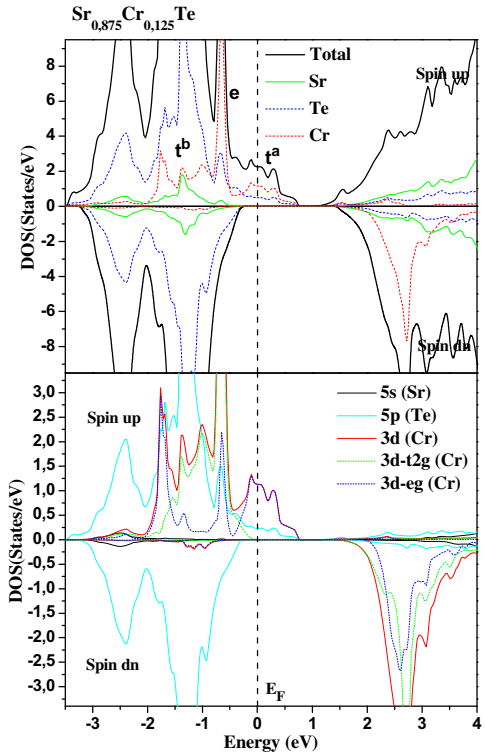

Fig. 10. Spin-polarized total and partial DOS of (5s) of Sr, (5p) of Te, and (3d, 3d-t_{2g}, 3d-e_g) of Cr in supercell of $Sr_{0.875}Cr_{0.125}Te$. The Fermi level is set to zero (vertical dotted line).

mean-field theory expressions [54,55]:

$$N_0\alpha = \frac{\Delta E_c}{x\langle s\rangle} \quad (1)$$

$$N_0\beta = \frac{\Delta E_v}{x\langle s\rangle} \quad (2)$$

where $\Delta E_c = E_c^{\downarrow} - E_c^{\uparrow}$ is the conduction band-edge spin-splitting and $\Delta E_v = E_v^{\downarrow} - E_v^{\uparrow}$ is the valence band-edge spin-splitting at the Γ symmetry point, (x) is the concentration of Cr, and $\langle s\rangle$ is half of the computed magnetization per Cr ion [54,55].

The calculated exchange constants $N_0\alpha$ and $N_0\beta$ for $Sr_{1-x}Cr_xZ$ (Z = S and Se) at concentrations $x = 0.0125$, 0.25, 0.5, 0.75 and $Sr_{1-x}Cr_xTe$ at $x = 0.0125$, 0.25, 0.5, 0.75, 0.875 are listed in Table 4. It shows that at all concentrations of Cr the exchange constants $N_0\alpha$ are positive whereas the $N_0\beta$ are negative. However, the exchange

interaction between the Cr spins and the electron carriers of conduction bands is explained by the $N_0\alpha$, while the $N_0\beta$ constants describe the exchange interaction between the Cr spins and the holes of valence bands. The negatives $N_0\beta$ and positives $N_0\alpha$ suggest the antiparallel and parallel spins, respectively. From our results, it is found that the anti-ferromagnetism and ferromagnetism are respectively attributed to the p-d exchange and s-d exchange coupling

4 Conclusion

The first-principles calculations of the density functional theory within the full-potential linearized augmented plane-wave method and generalized gradient approximation functional of Wu and Cohen were used to investigate the electronic and half-metallic ferromagnetic properties of $Sr_{1-x}Cr_xZ$ (Z = S, Se, and Te) at concentrations $x = 0.125$, 0.25, 0.5, 0.75, 0.875 in rock-salt phase. We reach that $Sr_{1-x}Cr_xZ$ (Z = S, Se, and Te) at $x = 0.125$, 0.25, 0.5, 0.75 and $Sr_{1-x}Cr_xTe$ at $x = 0.875$ exhibit a half-metallic ferromagnetic behavior with spin polarization of 100% at Fermi level, while the $Sr_{1-x}Cr_xS$ and $Sr_{1-x}Cr_xSe$ at $x = 0.875$ show a metallic feature. The ferromagnetic ground state is stable by the $3d$-e_g (Cr) partially filled states associated with the double-exchange mechanism, and it is found that $Sr_{1-x}Cr_xS$ at low concentration $x = 0.125$ depicts higher half-metallic gap of 0.815 eV compared with other compounds. Therefore, the $Sr_{0.875}Cr_{0.125}S$ is predicted to be a best promising candidate to explore half-metallic ferromagnetism for the practical applications of spintronic devices.

All authors contributed equally to this paper.

References

1. H. Ohno, Science **281**, 951 (1998)
2. S.A. Wolf, D.D. Awschalom, R.A. Buhrman, J.M. Daughton, S. von Molnár, M.L. Roukes, A.Y. Chtchelkanova, D.M. Treger, Science **294**, 1488 (2001)
3. I. Žutiæ, J. Fabian, S.D. Sarma, Rev. Mod. Phys. **76**, 323 (2004)
4. U.P. Verma, N. Devi, S. Sharma, P. Jensen, Eur. Phys. J. B **81**, 381 (2011)
5. Y. Huang, W. Jie, G. Zha, J. Alloys Compd. **539**, 271 (2012)
6. S.M. Alay-e-Abbas, K.M. Wong, N.A. Noor, A. Shaukat, Y. Lei, Solid State Sci. **14**, 1525 (2012)
7. B. Doumi, A. Tadjer, F. Dahmane, D. Mesri, H. Aourag, J. Supercond. Nov. Magn. **26**, 515 (2013)
8. Z.K. Tang, D.Y. Zhang, L.M. Tang, L.L. Wang, K.Q. Chen, Eur. Phys. J. B **86**, 284 (2013)
9. J.P. Tang, L.L. Wang, W.Z. Xiao, X.F. Li, Eur. Phys. J. B **86**, 362 (2013)
10. X. Dong, Q. Li, M. Xu, Eur. Phys. J. B **86**, 465 (2013)
11. M. Sajjad, H.X. Zhang, N.A. Noor, S.M. Alay-e-Abbas, A. Shaukat, Q. Mahmood, J. Magn. Magn. Mater. **343**, 177 (2013)
12. Z.Z. Wan, X.L. Wan, J.P. Liu, Q.B. Wang, J. Supercond. Nov. Magn. **27**, 1945 (2014)
13. M. Sajjad, H.X. Zhang, N.A. Noor, S.M. Alay-e-Abbas, M. Younas, M. Abid, A. Shaukat, J. Supercond. Nov. Magn. **27**, 2327 (2014)
14. L. Arda, M. Açıkgöz, A. Güngör, J. Supercond. Nov. Magn. **25**, 2701 (2012)
15. J. Singh, N.K. Verma, J. Supercond. Nov. Magn. **25**, 2425 (2012)
16. R.P. Borges, B. Ribeiro, M.M. Cruz, M. Godinho, U. Wahl, R.C. da Silva, A.P. Gonçalves, C. Magén, Eur. Phys. J. B **86**, 254 (2013)
17. F. Wang, W.W. Huang, S.Y. Li, A. Lian, X.T. Zhang, W. Cao, J. Magn. Magn. Mater. **340**, 5 (2013)
18. J. Singh, S. Kumar, N.K. Verma, Mater. Sci. Semicond. Proc. **26**, 1 (2014)
19. B. Babu, T. Aswani, G.T. Rao, R.J. Stella, B. Jayaraja, R.V.S.S.N. Ravikumar, J. Magn. Magn. Mater. **355**, 76 (2014)
20. B. Doumi, A. Tadjer, F. Dahmane, A. Djedid, A. Yakoubi, Y. Barkat, M. Ould Kada, A. Sayede, L. Hamada, J. Supercond. Nov. Magn. **27**, 293 (2014)
21. M. Kaminska, A. Twardowski, D. Wasik, J. Mater. Sci., Mater. Electron. **19**, 828 (2008)
22. A.L. Ruoff, T.A. Grzybowski, in *Solid State Physics Under Pressure*, edited by S. Minomura (Terra Scientific, Tokyo, 1985)
23. M. Dadsetani, A. Pourghazi, Phys. Rev. B **73**, 195102 (2006)
24. Y. Cheng, L.Y. Lu, O.H. Jia, X.R. Chen, Chin. Phys. B **17**, 1355 (2008)
25. L.Y. Lu, J.J. Tan, O.H. Jia, X.R. Chen, Physica B **399**, 66 (2007)
26. R. Pandey, S. Sivaraman, J. Phys. Chem. Solids **52**, 211 (1991)
27. N. Yamashita, T. Ohira, J. Phys. Soc. Jpn **53**, 419 (1984)
28. D. Varshney, N. Kaurav, R. Kinge, R.K. Singh, Comp. Mater. Sci. **41**, 529 (2008)
29. M. Yogeswari, G. Kalpana, Comp. Mater. Sci. **54**, 219 (2012)
30. M. Yogeswari, R. Umamageshwari, G. Kalpana, Comp. Mater. Sci. **65**, 426 (2012)
31. M. Yogeswari, G. Kalpana, J. Alloys Compd. **573**, 83 (2013)
32. Z. Wu, R.E. Cohen, Phys. Rev. B **73**, 235116 (2006)
33. P. Hohenberg, W. Kohn, Phys. Rev. **136**, B864 (1964)
34. W. Kohn, L.J. Sham, Phys. Rev. **140**, A1133 (1965)
35. P. Blaha, K. Schwarz, G.K.H. Madsen, D. Kvasnicka, J. Luitz, WIEN2K Vienna University of Technology, Austria (2001)
36. K. Syassen, Phys. Stat. Sol. A **91**, 11 (1985)
37. H. Luo, R.G. Greene, A.L. Ruoff, Phys. Rev. B **49**, 15341 (1994)
38. H.G. Zimmer, H. Winzen, K. Syassen, Phys. Rev. B **32**, 4066 (1985)
39. H.J. Monkhorst, J.D. Pack, Phys. Rev. B **13**, 5188 (1976)
40. J.D. Pack, H.J. Monkhorst, Phys. Rev. B **16**, 1748 (1977)
41. F.D. Muranghan, Proc. Natl. Acad. Sci. USA **30**, 244 (1944)
42. M. Souadkia, B. Bennecer, F. Kalarasse, A. Mellouki, Comput. Mater. Sci. **50**, 1701 (2011)

43. S. Labidi, H. Meradji, S. Ghemid, M. Labidi, F. El Haj Hassan, J. Phys.: Condens. Matter **20**, 445213 (2008)
44. J.P. Perdew, K. Burke, M. Ernzerhof, Phys. Rev. Lett. **77**, 3865 (1996)
45. S. Sharma, A.S. Verma, R. Bhandari, S. Kumari, V.K. Jindal, Mater. Sci. Semicond. Proc. **27**, 79 (2014)
46. M. Sajjad, S. Manzoor, H.X. Zhang, N.A. Noor, S.M. Alaye-Abbas, A. Shaukat, R. Khenata, J. Magn. Magn. Mater. **379**, 63 (2015)
47. B. Doumi, A. Mokaddem, M. Ishak-Boushaki, D. Bensaid, Mater. Sci. Semicond. Proc. **32**, 166 (2015)
48. K.L. Yao, G.Y. Gao, Z.L. Liu, L. Zhu, Solid State Commun. **133**, 301 (2005)
49. G.Y. Gao, K.L. Yao, E. Şaşıoğlu, L.M. Sandratskii, Z.L. Liu, J.L. Jiang, Phys. Rev. B **75**, 174442 (2007)
50. H. Akai, Phys. Rev. Lett. **81**, 3002 (1998)
51. K. Sato, H. Katayama-Yoshida, Semicond. Sci. Technol. **17**, 367 (2002)
52. K. Sato, P.H. Dederichs, K. Araki, H. Katayama-Yoshida, Phys. Stat. Sol. C **7**, 2855 (2003)
53. K. Sato, H. Katayama-Yoshida, P.H. Dederichs, J. Supercond. **16**, 31 (2003)
54. S. Sanvito, P. Ordejon, N.A. Hill, Phys. Rev. B **63**, 165206 (2001)
55. H. Raebiger, A. Ayuela, R.M. Nieminen, J. Phys.: Condens. Matter **16**, L457 (2004)